Cite as: B. Bahari *et al.*, *Science* 10.1126/science.aao4551 (2017).

Nonreciprocal lasing in topological cavities of arbitrary geometries

Babak Bahari, Abdoulaye Ndao, Felipe Vallini, Abdelkrim El Amili, Yeshaiahu Fainman, Boubacar Kanté*

Department of Electrical and Computer Engineering, University of California, San Diego, La Jolla, CA 92093, USA.

*Corresponding author. Email: bkante@ucsd.edu

Resonant cavities are essential building blocks governing many wave based phenomena, and, their geometry together with reciprocity, fundamentally limit the integration of optical devices. We report, at telecommunication wavelengths, geometry-independent and integrated nonreciprocal topological cavities that couple stimulated emission from one-way photonic edge states to a selected waveguide output with an isolation ratio in excess of 10 dB. Nonreciprocity originates from unidirectional edge states at the boundary between photonic structures with distinct topological invariants. Our experimental demonstration of lasing from topological cavities provides the opportunity to develop complex topological circuitry of arbitrary geometries for the integrated and robust generation and transport of photons in classical and quantum regimes.

Soon after the advent of quantum mechanics, Bloch established the theory of the electronic band structure of solids (electrons are fermions), resulting in the classification of materials as either electrical conductors or insulators (*1*). It was later understood that the band structure of fermionic systems obeys a more sophisticated classification beyond Landau's spontaneous symmetry breaking theory (*2*). Fermionic materials known as topological insulators are insulators in their bulk but conductors at their interfaces. Topological classifications can be extended to bosonic systems, namely photonic crystals (*3*, *4*), which also possess a band structure obeying Bloch's theorem (*5*, *6*). Experimental demonstration of robust electromagnetic transport in microwaves followed (*7*) and topological order has since been shown to be ubiquitous in many areas of wave physics including microwaves, acoustics, excitonics, and plasmonics (*8*–*17*). However, demonstrations in systems with broken time-reversal symmetry, have until now been limited to the passive topological transport of electromagnetic waves at low frequencies. Proposals to increase the operating frequency from microwaves to terahertz and the optical regime have been put forward for various platforms with and without time-reversal symmetry breaking (*18*–*23*). Topological lasing has been proposed in two dimensions using arrays of ring resonators with no time-reversal symmetry breaking (*24*), in one-dimensional resonant periodic crystals (*25*), and in one-dimensional lattice of polariton micropillars that implements an orbital version of the Su-Schrieer-Heeger Hamiltonian (*26*). However, these systems cannot implement cavities of arbitrary shapes due to their preserved time-reversal symmetry (*27*). An elusive implication of topology is the existence of a new class of geometry-independent photonic components. For example, the possibility to construct geometry-independent cavities (*28*, *29*) opens a new paradigm in cavity quantum electro dynamics and photonic integration as it enables denser packing of components and sources of arbitrary form-factors. Realizing this prospect would alleviate the constraints to use preset cavities that leave much chip space unused. Topology also naturally addresses the pressing need for nonreciprocal components that protect sources against back scattering.

We report on the nonreciprocal single mode lasing from topological cavities of arbitrary geometries operating at room temperature and at telecommunication wavelengths. The integrated nonreciprocal topological cavities, using a static magnetic field to break time-reversal symmetry, couple stimulated emission from one-way photonic edge states to a selected waveguide output with an isolation ratio in excess of 10 dB. The proposed platform opens perspectives in integrated photonics, in which, information can robustly flow between sectors characterized by different topological indices.

Our topological cavity platform (Fig. 1), is made of arbitrarily-shaped closed contours that constitute the cavity and a waveguide to which the cavity is evanescently coupled. The structures are made of structured InGaAsP multiple quantum wells, bonded on Yttrium Iron Garnet (YIG) a gyrotropic material grown on Gadolinium Gallium Garnett (GGG) by molecular beam epitaxy. The YIG substrate is used to break time-reversal symmetry in the system under a static External Magnetic Field (EMF). The closed contour (cavity) is defined by two different Photonic Crystals (PhCs). The

PhC enclosed by the cavity (inside the contour) is a square lattice with a star-shaped unit cell. The PhC not enclosed by the contour constitutes the rest of the system, and, it is made of a triangular lattice with cylindrical air holes unit cell. A defect waveguide coupled to the cavity is created by removing a line of air holes in the PhC with triangular lattice. Distinct topological invariants of the two PhCs will ensure the existence of robust one-way edge states at their interface, creating a one-way topological cavity that will couple its emission either to the right or the left output of the waveguide depending on the direction of the EMF. For example, a counterclockwise topological edge state, as shown in Fig. 1, will preferentially couple its emission to the right output of the waveguide.

Band diagrams of the two PhCs are calculated using finite-element method. Fig. 2A presents the band diagram of the square lattice PhC in presence of an EMF $\mathbf{B} = B_0\mathbf{e}_z$, with $B_0 = +100$ Oe. This magnetic field saturates the YIG material, maximizing the nondiagonal components of its dielectric permittivity tensor (*30*, *31*). Initially, the EMF is zero, and, the band structure does not exhibit any gap in the frequency range of interest. Application of the EMF ($+B_0$) opens a narrow band gap (green shaded region in Fig. 2A) with a width of $\Delta\lambda \sim 42$ pm. The sum of the topological invariant, also known as Chern number (*4*, *7*), associated with each bulk mode below the corresponding band gap is $|\Sigma C| = 1$ (*31*). This band gap is called nontrivial band gap because of the nonzero sum of the Chern numbers (*4*). It is worth noting that, while the small nontrivial gap (restricted by the gyromagnetism strength of materials at optical frequencies) put a limitation on some applications, it provides sufficient feedback for lasing cavities.

One-way interfaces can be implemented using another PhC with a different topological invariant (Fig. 2B). Here, the PhC with triangular lattice possesses a broad band gap regardless of the amplitude of the EMF and in particular for the value of EMF used for the nontrivial PhC. Calculations indicate a zero sum of Chern numbers for modes below this gap that is thus called trivial band gap (*31*). The dispersion of the one-way edge state at the interface between the two PhCs is presented in (*31*). Dimensions of the two PhCs have been chosen to overlap their band gaps around the telecommunication wavelength of $\lambda \sim 1.5$ μm, where the gain of InGaAsP material peaks. The closed contour between the trivial and nontrivial photonic structures constitutes the topological cavity that, in principle, can have arbitrary geometries while maintaining its resonant frequency. The dissimilar topology of the two band gaps is numerically verified in Fig. 2, C and D. A point source, with a wavelength in the band gap of the two crystals, is placed at the interface between the two PhCs. The energy of the source is confined at the interface and propagates to the right for an EMF of $+B_0\mathbf{e}_z$ (Fig. 2C). By reversing the direction of the EMF ($-B_0\mathbf{e}_z$) the propagation to the right is forbidden, demonstrating the existence of a one-way edge state.

To demonstrate the versatility of the proposed platform, we first investigate a square cavity coupled to the waveguide. The total length of the nontrivial cavity and the coupling length between the cavity and the waveguide were optimized for the edge mode (*31*). The structure is fabricated by electron beam lithography followed by dry etching to form the trivial and nontrivial PhCs. The PhCs are subsequently bonded on a flat YIG substrate coated with a thin layer of polymethyl methacrylate. Finally, the InP substrate, on which InGaAsP is epitaxially grown, is removed by wet etching using hydrochloric acid (*31*). Figure 3A presents a top view Scanning Electron Micrograph (SEM) of a fabricated device where the trivial and nontrivial PhCs together with the waveguide can be seen. The fabrication is uniform over the entire area of the device.

The devices are optically pumped from the top with a pulsed laser ($\lambda_{pump} = 1064$ nm, T = 12 ns pulse at a repetition rate f = 275 kHz) using a micro photoluminescence setup. The size of the pump beam is controlled to cover the whole area of the device. Figure 3, B and C, represent real space camera images of the surface of the devices without ($B_0 = 0$) and with ($B_0 = +100$ Oe) EMF respectively, for a pump power density of $\rho = 0.9$ μW/μm². An edge mode, localized at the interface between the two PhCs is observed in the presence of the EMF (Fig. 3C) while it disappears when the EMF is turned off (Fig. 3B).

To further characterize the device and demonstrate the unidirectionality of the edge mode, a lensed fiber is coupled to one of the outputs of the waveguide. The outputs of the waveguides are tapered to ensure efficient coupling to the fiber. The coupling was aided by a piezoelectric positioning device with nanometer resolution. The tip of the lensed fiber is placed in front of the waveguide and the other end of the fiber is directly connected to an optical spectrum analyzer.

Figure 3D shows the evolution of the output power as a function of both pump power density and wavelength. By varying the pump power density with the EMF turned on, a threshold behavior with a clear transition from spontaneous emission to stimulated emission (lasing) is observed. Turning off the EMF results in the suppression of lasing (*31*).

To prove that lasing is from a one-way edge mode, we flipped the direction of the EMF by reversing the current in the solenoid creating $\mathbf{B} = -B_0\mathbf{e}_z$ and measured the emitted power and its spectrum. This is equivalent to coupling the fiber to the other end of the waveguide for a fixed direction of the EMF, with the advantage of avoiding discrepancies between the coupling efficiencies to the two ends of the waveguide, thus enabling quantitative comparison of the

emissions.

Figure 3E presents the output emission power of the structure for two opposite values of the EMF ($+B_0$ and $-B_0$) for the same pump power density (ρ = 0.9 $\mu W/\mu m^2$) in the lasing regime. As seen, there is a large reduction in the luminescence spectrum and an isolation ratio of 9.85 dB is measured. In nontopological cavities with broken time-reversal symmetry (that cannot have arbitrary shapes), the Clock-Wise (CW) and the Counter Clock-Wise (CCW) modes of the cavity have similar characteristics, but a small wavelength shift (*30*). However, in topological cavities, one of the modes, either the CW or the CCW is forbidden depending on the direction of EMF, and thus, cannot be excited, ensuring single mode operation. This is a fundamental difference between these systems, as nontopological cavities will exhibit two slightly detuned modes that both lay within the broad gain bandwidth of the semiconductor and would thus give rise to mode competition.

Topological edge modes are robust against backscattering from imperfections and sharp corners. Beyond robust and passive transport, this implies the possibility to implement deformed cavities of arbitrary geometries. Figure 4A shows the top view SEM of an arbitrarily-shaped cavity with a geometry approximating a flipped USA-like map with the same optical length as the square cavity. We optically pump the device from the top, collect and analyze the emission from the tapered waveguide using the lensed fiber again. When the EMF is turned on, real space imaging of the top of the device (Fig. 4B) provides evidence for an edge mode that is tightly confined at the boundary of the topologically distinct photonic structures. When EMF is turned off, the edge mode disappears (Fig. 4D). Unidirectional lasing with an isolation ratio of 11.3 dB is experimentally achieved with a pump power density of ρ = 0.9 $\mu W/\mu m^2$ (see Fig. 4C). Additional deformed cavities of different shapes are presented (*31*).

We experimentally demonstrated nonreciprocal lasing from topological cavities of arbitrary geometries. The topological cavities are closed contours between photonic structures with distinct topological invariants and thus support unidirectional edge states circulating around the cavity. The topologically distinct structures are made from two photonic crystals with overlapping trivial and nontrivial band gaps at telecommunication wavelengths. By evanescently coupling a waveguide to the topological cavity, stimulated emission from the one-way mode is coupled to a selected waveguide output with an isolation ratio as large as 11.3 dB. Cavities are implemented on structured InGaAsP, the semiconductor providing optical gain, bonded on a YIG substrate that breaks time-reversal symmetry in the devices. These results demonstrate the flexibility of topological cavities and open avenues in photonic integration where information can robustly flow between sectors characterized by their topological invariants and will enable the investigation of nontrivial photonic devices.

REFERENCES AND NOTES

1. N. W. Ashcroft, N. D. Mermin, *Solid State Physics* (Holt, Rinehart and Winston, 1976).
2. M. Z. Hasan, C. L. Kane, Colloquium: Topological insulators. *Rev. Mod. Phys.* **82**, 3045–3067 (2010). doi:10.1103/RevModPhys.82.3045
3. F. D. M. Haldane, S. Raghu, Possible realization of directional optical waveguides in photonic crystals with broken time-reversal symmetry. *Phys. Rev. Lett.* **100**, 013904 (2008). doi:10.1103/PhysRevLett.100.013904 Medline
4. S. Raghu, F. D. M. Haldane, Analogs of quantum-Hall-effect edge states in photonic crystals. *Phys. Rev. A* **78**, 033834 (2008). doi:10.1103/PhysRevA.78.033834
5. E. Yablonovitch, Inhibited spontaneous emission in solid-state physics and electronics. *Phys. Rev. Lett.* **58**, 2059–2062 (1987). doi:10.1103/PhysRevLett.58.2059 Medline
6. S. John, Strong localization of photons in certain disordered dielectric superlattices. *Phys. Rev. Lett.* **58**, 2486–2489 (1987). doi:10.1103/PhysRevLett.58.2486 Medline
7. Z. Wang, Y. Chong, J. D. Joannopoulos, M. Soljacić, Observation of unidirectional backscattering-immune topological electromagnetic states. *Nature* **461**, 772–775 (2009). doi:10.1038/nature08293 Medline
8. Y. Poo, R. X. Wu, Z. Lin, Y. Yang, C. T. Chan, Experimental realization of self-guiding unidirectional electromagnetic edge states. *Phys. Rev. Lett.* **106**, 093903 (2011). doi:10.1103/PhysRevLett.106.093903 Medline
9. M. C. Rechtsman, J. M. Zeuner, A. Tunnermann, S. Nolte, M. Segev, A. Szameit, Strain-induced pseudomagnetic field and photonic Landau levels in dielectric structures. *Nat. Photonics* **7**, 153–158 (2012). doi:10.1038/nphoton.2012.302
10. A. B. Khanikaev, S. H. Mousavi, W.-K. Tse, M. Kargarian, A. H. MacDonald, G. Shvets, Photonic topological insulators. *Nat. Mater.* **12**, 233–239 (2013). doi:10.1038/nmat3520 Medline
11. Y.-J. Chen, S.-J. Jiang, X.-D. Chen, B. Zhu, L. Zhou, J.-W. Dong, C. T. Chan, Experimental realization of photonic topological insulator in a uniaxial metacrystal waveguide. *Nat. Commun.* **5**, 5782 (2014). doi:10.1038/ncomms6782
12. X. Cheng, C. Jouvaud, X. Ni, S. H. Mousavi, A. Z. Genack, A. B. Khanikaev, Robust reconfigurable electromagnetic pathways within a photonic topological insulator. *Nat. Mater.* **15**, 542–548 (2016). doi:10.1038/nmat4573 Medline
13. A. P. Slobozhanyuk, A. B. Khanikaev, D. S. Filonov, D. A. Smirnova, A. E. Miroshnichenko, Y. S. Kivshar, Experimental demonstration of topological effects in bianisotropic metamaterials. *Sci. Rep.* **6**, 22270 (2016). doi:10.1038/srep22270 Medline
14. A. B. Khanikaev, R. Fleury, S. H. Mousavi, A. Alù, Topologically robust sound propagation in an angular-momentum-biased graphene-like resonator lattice. *Nat. Commun.* **6**, 8260 (2015). doi:10.1038/ncomms9260 Medline
15. R. Fleury, A. B. Khanikaev, A. Alù, Floquet topological insulators for sound. *Nat. Commun.* **7**, 11744 (2016). doi:10.1038/ncomms11744 Medline
16. J. Yuen-Zhou, S. K. Saikin, N. Y. Yao, A. Aspuru-Guzik, Topologically protected excitons in porphyrin thin films. *Nat. Mater.* **13**, 1026–1032 (2014). doi:10.1038/nmat4073 Medline
17. D. Jin, T. Christensen, M. Soljačić, N. X. Fang, L. Lu, X. Zhang, Infrared topological

plasmons in graphene. *Phys. Rev. Lett.* **118**, 245301 (2017). doi:10.1103/PhysRevLett.118.245301 Medline

18. B. Bahari, R. Tellez-Limon, B. Kanté, Topological terahertz circuits using semiconductors. *Appl. Phys. Lett.* **109**, 143501 (2016). doi:10.1063/1.4963789
19. M. C. Rechtsman, J. M. Zeuner, Y. Plotnik, Y. Lumer, D. Podolsky, F. Dreisow, S. Nolte, M. Segev, A. Szameit, Photonic Floquet topological insulators. *Nature* **496**, 196–200 (2013). doi:10.1038/nature12066 Medline
20. M. Hafezi, S. Mittal, J. Fan, A. Migdall, J. M. Taylor, Imaging topological edge states in silicon photonics. *Nat. Photonics* **7**, 1001–1005 (2013). doi:10.1038/nphoton.2013.274
21. Y. Plotnik, M. C. Rechtsman, D. Song, M. Heinrich, J. M. Zeuner, S. Nolte, Y. Lumer, N. Malkova, J. Xu, A. Szameit, Z. Chen, M. Segev, Observation of unconventional edge states in 'photonic graphene'. *Nat. Mater.* **13**, 57–62 (2014). doi:10.1038/nmat3783 Medline
22. A. P. Slobozhanyuk, A. N. Poddubny, A. E. Miroshnichenko, P. A. Belov, Y. S. Kivshar, Subwavelength topological edge states in optically resonant dielectric structures. *Phys. Rev. Lett.* **114**, 123901 (2015). doi:10.1103/PhysRevLett.114.123901 Medline
23. A. Slobozhanyuk, S. H. Mousavi, X. Ni, D. Smirnova, Y. S. Kivshar, A. B. Khanikaev, Three-dimensional all-dielectric photonic topological insulator. *Nat. Photonics* **11**, 130–136 (2016). doi:10.1038/nphoton.2016.253
24. S. Wittek, G. Harari, M. A. Bandres, H. Hodaei, M. Parto, P. Aleahmad, M. C. Rechtsman, Y. D. Chong, D. N. Christodoulides, M. Khajavikhan, M. Segev, in *Conference on Lasers and Electro-Optics, OSA Technical Digest* (Optical Society of America, 2017), paper FTh1D.3.
25. L. Pilozzi, C. Conti, Topological lasing in resonant photonic structures. *Phys. Rev. B* **93**, 195317 (2016). doi:10.1103/PhysRevB.93.195317
26. P. St-Jean, V. Goblot, E. Galopin, A. Lemaitre, T. Ozawa, L. Le Gratiet, I. Sagnes, J. Bloch, A. Amo, Lasing in topological edge states of a 1D lattice. arXiv:1704.07310 (2017).
27. J. Noh, S. Huang, K. Chen, M. C. Rechtsman, Observation of photonic topological valley-Hall edge state. arXiv:1706.00059 (2017).
28. I. Liberal, A. M. Mahmoud, N. Engheta, Geometry-invariant resonant cavities. *Nat. Commun.* **7**, 10989 (2016). doi:10.1038/ncomms10989 Medline
29. T. Ma, G. Shvets, All-Si valley-Hall photonic topological insulator. *New J. Phys.* **18**, 025012 (2016). doi:10.1088/1367-2630/18/2/025012
30. L. Bi, J. Hu, P. Jiang, D. H. Kim, G. F. Dionne, L. C. Kimerling, C. A. Ross, On-chip optical isolation in monolithically integrated non-reciprocal optical resonators. *Nat. Photonics* **5**, 758–762 (2011). doi:10.1038/nphoton.2011.270
31. See supplementary materials.
32. B. E. A. Saleh, M. C. Teich, *Fundamentals of Photonics* (Wiley, ed. 2, 2007), chap. 20.

ACKNOWLEDGMENTS

This research was partially supported by the Office of Naval Research Young Investigator Award (N00014-17-1-2671), the National Science Foundation Career Award (ECCS-1554021), the U.S. Department of Energy (EE0007341), the National Science Foundation (ECCS-1405234, ECCS-1507146, CCF-1640227), the Office of Naval Research Multi-University Research Initiative (N00014-13-1-0678), the Army Research Office (W911NF-16-1-0245), the Semiconductor Research Corporation, and the startup funds provided to B.K. by the University of California San Diego. The work was performed in part at the San Diego Nanotechnology Infrastructure, a member of the National Nanotechnology Coordinated Infrastructure, which is supported by the National Science Foundation (ECCS-1542148). We thank Dr. Maria Isabel Montero Ramirez for technical assistance regarding electron beam lithography and Dr. Thomas Lepetit for helpful discussions. The Regents of the University of California filed a patent on systems and applications using devices based on topological cavities.

SUPPLEMENTARY MATERIALS

www.sciencemag.org/cgi/content/full/science.aao4551/DC1
Supplementary Text
Figs. S1 to S11
Reference (*32*)

22 July 2017; accepted 28 September 2017
Published online 12 October 2017
10.1126/science.aao4551

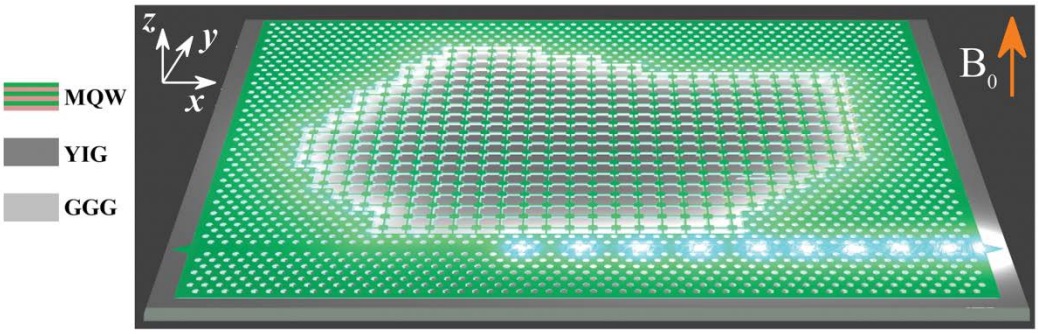

Fig. 1. Principle of an arbitrarily-shaped and integrated topological cavity. The topological cavity is an arbitrarily-shaped closed contour formed between the boundaries of two photonic structures with distinct topological invariants. The structures are made of InGaAsP multiple quantum wells (MQW), bonded on Yttrium Iron Garnet (YIG) grown on Gadolinium Gallium Garnett (GGG) by molecular beam epitaxy. The YIG substrate is used to break time reversal symmetry in the system under a static External Magnetic Field (EMF). The Photonic Crystal (PhC) enclosed by the cavity (inside the contour) is a square lattice with a star-shaped unit cell. The photonic crystal not enclosed by the contour constitutes the rest of the system, and, is made of a triangular lattice with cylindrical air holes unit cell. A defect waveguide is evanescently coupled to the cavity, and is created by removing a line of air holes in the PhC with a triangular lattice. The topological one-way edge state circulating around the cavity is evanescently coupled to the defect waveguide resulting in emission at one output of the waveguide. The direction of emission can be reversed by flipping the sign of the EMF. For example, under an EMF and optical pumping from the top of the device, a counterclockwise topological edge state will preferentially couple its emission to the right output of the waveguide. Light from the tapered waveguide is then collected and analyzed using a lensed fiber connected to an optical spectrum analyzer.

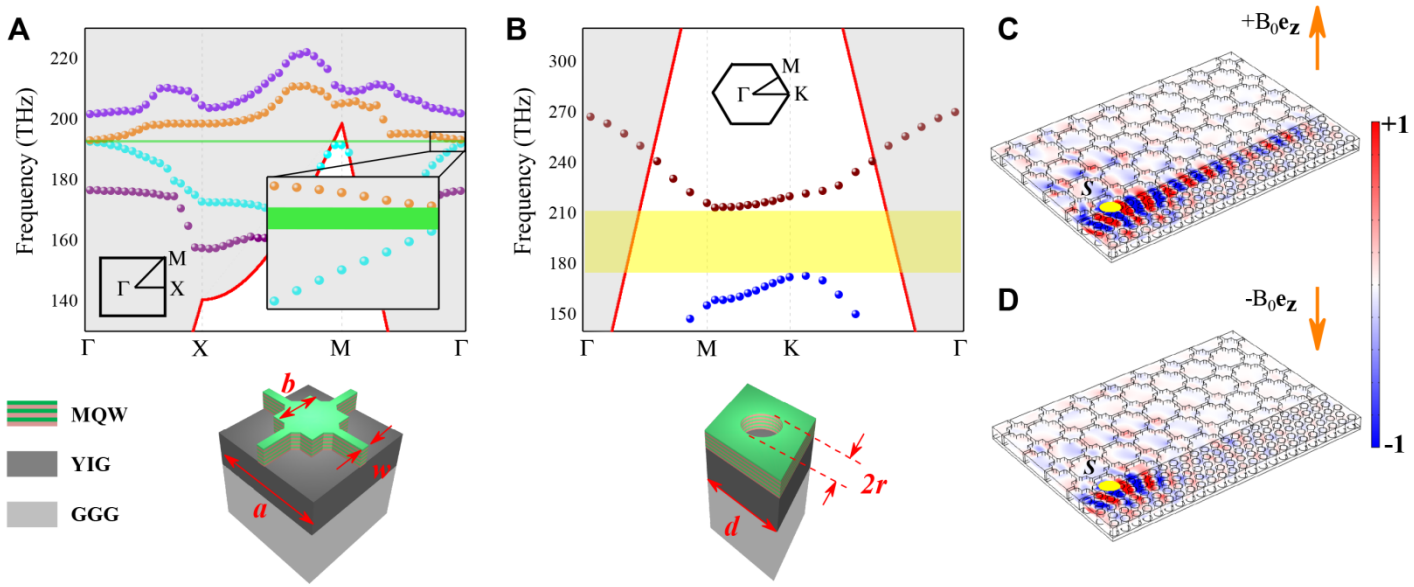

Fig. 2. Design of the nontrivial and trivial photonic structures and full-wave simulation of the edge mode. (**A**) Photonic band diagram of a star-shaped Photonic Crystal (PhC) with a unit cell shown at the bottom. The PhC is made of InGaAsP material and it has a square lattice with dimensions a = 1084 nm (period), b = 0.46a, and w = 0.0844a. The band diagram of the square lattice PhC is calculated in presence of an EMF that saturates the YIG material, and thus maximizes the nondiagonal component of its dielectric permittivity tensor. Initially, the EMF is zero and the band structure does not exhibit any gap in the frequency range of interest (not shown). The application of the EMF ($+B_0$) opens a narrow band gap (green shaded region) with a width of $\Delta\lambda \sim 42$ pm. The sum of the topological invariant, also known as Chern number (*4*, *7*), associated with each bulk mode below the corresponding band gap is $|\Sigma C| = 1$ (*31*). Red solid lines represent the light-cone. (**B**) Photonic band diagram of a triangular lattice PhC with cylindrical air holes unit cell (shown at the bottom) in presence of the same EMF as in (A). The periodicity d and radius of holes r are $a/3$ and 0.35d, respectively. A broad band gap is obtained, almost independent of the amplitude of the EMF. Calculations indicate zero for the sum of the Chern numbers of modes below this gap (*31*). The boundary between these two PhCs with overlapping band gaps thus supports one-way edge states that propagate either to the right (**C**) or to the left (**D**) depending on the direction of the EMF. In the two cases, the thickness of the InGaAsP and YIG are 300 nm and 200 nm, respectively. Band diagrams are calculated along their respective irreducible Brillouin zones.

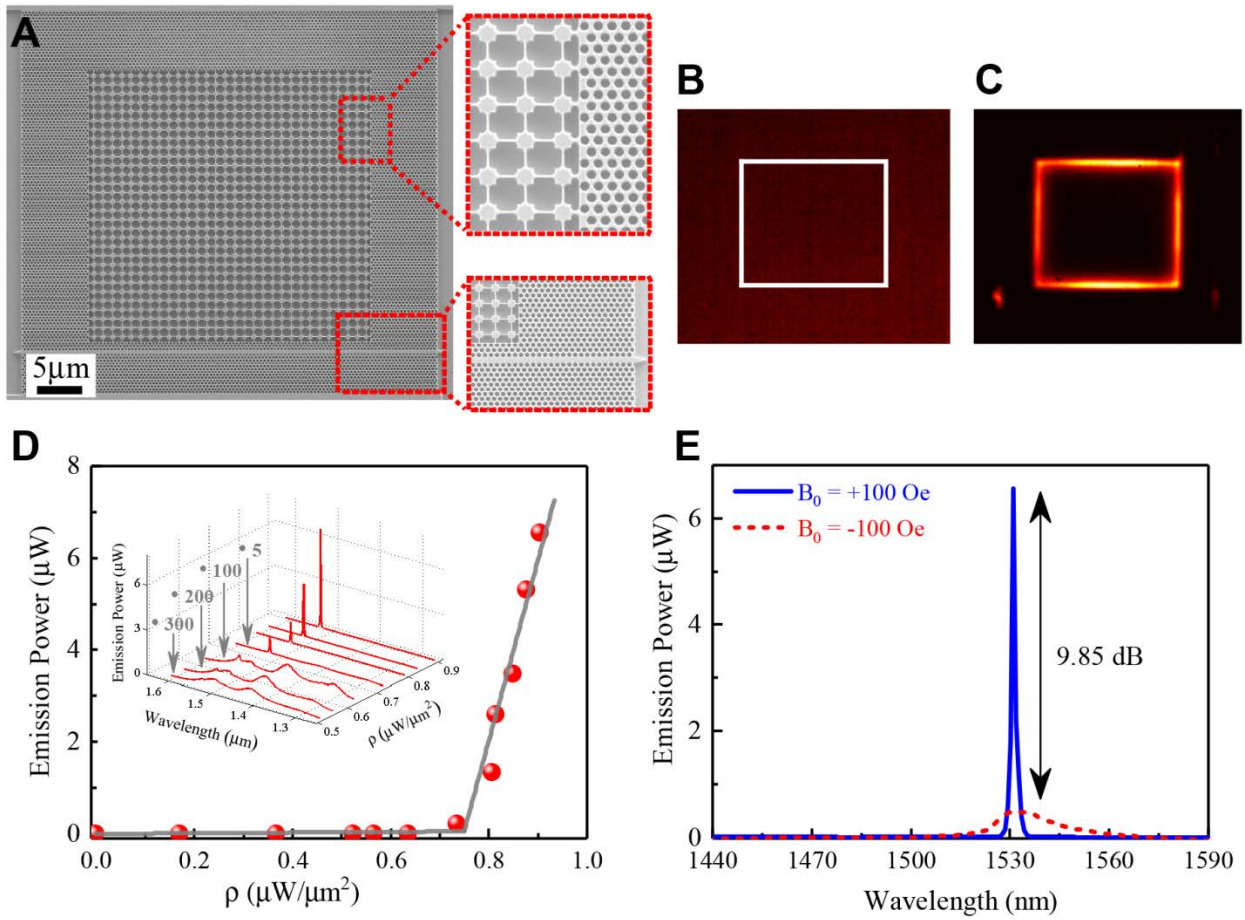

Fig. 3. Experimental evidence of the edge mode and unidirectional lasing from a square-shaped topological cavity. (**A**) Top view Scanning Electron Micrograph (SEM) of a fabricated squared-shaped topological cavity where the trivial and nontrivial PhCs together with the waveguide can be seen. Structures are fabricated on InGaAsP by electron beam lithography followed by dry etching and then bonded on a YIG substrate with a thin layer of polymethyl methacrylate. The InP substrate, on which InGaAsP is epitaxially grown, is subsequently removed by wet etching using hydrochloric acid (*31*). Real space camera images of the top of the device without (**B**) and with (**C**) EMF under optical pumping using a 1064 nm wavelength laser. Unambiguously, an edge mode, localized at the interface between the two PhCs is observed in the presence of the EMF while it disappears when the EMF is turned off. (**D**) Evolution of the output power collected by a lensed fiber coupled to the output of the waveguide as a function of pump power density and wavelength. Red dots are experimental measurements of the output power for different pump power densities when the EMF is turned on. Gray solid lines are linear fits to the data in spontaneous and stimulated emission regimes and clearly show a threshold behavior, *i.e.*, lasing. No lasing is observed in the absence of EMF (*31*). (**E**) Emission power for a pump power density of $\rho = 0.9\mu W/\mu m^2$ (lasing regime) for two opposite values of the EMF ($+B_0$ and $-B_0$), which is equivalent to collecting emission from the two outputs of the waveguide with the advantage of avoiding coupling discrepancies. An isolation ratio of 9.85 dB is experimentally observed, confirming nonreciprocal lasing.

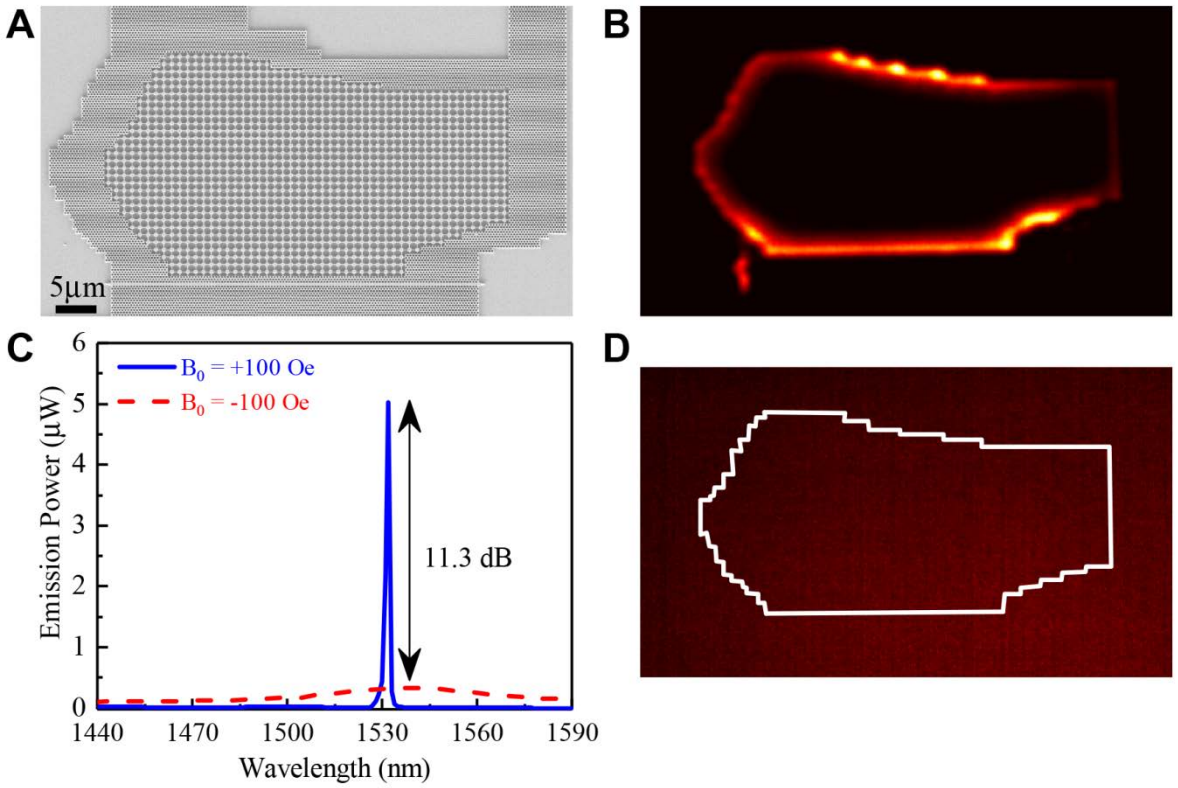

Fig. 4. Geometry-independent cavity and nonreciprocal lasing. (**A**) Top view SEM of a fabricated arbitrarily-shaped topological cavity with a geometry approximating a flipped USA-like map. The structure is fabricated using the same process as in Fig. 3. The shape of the cavity is deformed to investigate geometry-independence of the topological cavities while the optical length is the same as in the cavity of Fig. 3. The coupling length between the cavity and the waveguide is also unchanged. (**B**) Real space camera image of the top of the device under high power optical pumping (ρ = 0.9μW/μm^2 at λ_{pump} = 1064nm) and with the EMF turned on. An edge mode that is confined at the boundary of the topologically distinct photonic structures is clearly observed. (**C**) Photoluminescence spectrum of the topological cavity for two opposite values of the EMF for a pump power density of ρ = 0.9μW/μm^2 (lasing regime). As shown, for a forward bias (+B_0), the cavity lases with stimulated emission, but for a backward bias (-B_0), a strong suppression of emission is obtained with an isolation ratio between ports of 11.3 dB. (**D**) The edge mode disappears when the EMF is turned off because the nontrivial band gap closes.

Nonreciprocal lasing in topological cavities of arbitrary geometries

Babak Bahari, Abdoulaye Ndao, Felipe Vallini, Abdelkrim El Amili, Yeshaiahu Fainman and Boubacar Kanté

published online October 12, 2017